

ENVIRONMENTAL RESEARCH CLIMATE



PAPER

Ultrafast Arctic amplification and its governing mechanisms






OPEN ACCESS

RECEIVED
10 November 2022

REVISED
21 June 2023

ACCEPTED FOR PUBLICATION
27 June 2023

PUBLISHED
11 July 2023

Tyler P Janoski^{1,2,*} , Michael Previdi³ , Gabriel Chiodo³ , Karen L Smith^{2,4}  and Lorenzo M Polvani^{1,2,5} 

¹ Department of Earth and Environmental Sciences, Columbia University, New York, NY, United States of America

² Lamont-Doherty Earth Observatory, Palisades, NY, United States of America

³ Institute for Atmospheric and Climate Science, ETH Zürich, Zürich, Switzerland

⁴ Department of Physical and Environmental Sciences, University of Toronto Scarborough, Scarborough, ON, Canada

⁵ Department of Applied Physics and Applied Mathematics, Columbia University, New York, NY, United States of America

* Author to whom any correspondence should be addressed.

E-mail: janoski@ldeo.columbia.edu

Original content from this work may be used under the terms of the [Creative Commons Attribution 4.0 licence](https://creativecommons.org/licenses/by/4.0/).

Any further distribution of this work must maintain attribution to the author(s) and the title of the work, journal citation and DOI.



Keywords: Arctic amplification, sea ice, heat transport, turbulent heat flux, radiative feedback

Supplementary material for this article is available [online](#)

Abstract

Arctic amplification (AA), defined as the enhanced warming of the Arctic compared to the global average, is a robust feature of historical observations and simulations of future climate. Despite many studies investigating AA mechanisms, their relative importance remains contested. In this study, we examine the different timescales of these mechanisms to improve our understanding of AA's fundamental causes. We use the Community Earth System Model v1, Large Ensemble configuration (CESM-LE), to generate large ensembles of 2 years simulations subjected to an instantaneous quadrupling of CO₂. We show that AA emerges almost immediately (within days) following CO₂ increase and before any significant loss of Arctic sea ice has occurred. Through a detailed energy budget analysis of the atmospheric column, we determine the time-varying contributions of AA mechanisms over the simulation period. Additionally, we examine the dependence of these mechanisms on the season of CO₂ quadrupling. We find that the surface heat uptake resulting from the different latent heat flux anomalies between the Arctic and global average, driven by the CO₂ forcing, is the most important AA contributor on short (<1 month) timescales when CO₂ is increased in January, followed by the lapse rate feedback. The latent heat flux anomaly remains the dominant AA mechanism when CO₂ is increased in July and is joined by the surface albedo feedback, although AA takes longer to develop. Other feedbacks and energy transports become relevant on longer (>1 month) timescales. Our results confirm that AA is an inherently fast atmospheric response to radiative forcing and reveal a new AA mechanism.

1. Introduction

Arctic amplification (AA), or the enhanced surface warming of the Arctic relative to the global mean, is a ubiquitous feature of anthropogenic climate change. First predicted by Arrhenius in 1896 as a response to increasing CO₂ (Arrhenius 1896), AA has since consistently appeared in climate model simulations (e.g., Manabe and Stouffer 1980, Hwang *et al* 2011, Pithan and Mauritsen 2014) and observations (e.g., Serreze *et al* 2009, Cohen *et al* 2014, Wang *et al* 2016). The local and global importance of AA cannot be overstated. The Arctic is home to ~4 million people, including indigenous peoples who have lived there for 20 000 years (National Snow and Ice Data Center 2020). Amplified Arctic warming threatens these peoples' ways of life while simultaneously endangering the surrounding Arctic ecosystems (Melfoite *et al* 2013, Moon *et al* 2021). Impacts of AA are not limited to the Arctic; a warmer Arctic may lead to the release of methane, a potent greenhouse gas, from permafrost (Zubrzycki *et al* 2014) and may influence extreme weather in the midlatitudes (Francis and Vavrus 2012, Cohen *et al* 2014, Smith *et al* 2022). There may, however, be some benefits to global shipping and agriculture from Arctic warming (Ho 2010, Altdorff *et al* 2021).

Despite AA's ubiquity, the question of the mechanisms to which AA owes its existence remains open, limiting our ability to understand and accurately project future Arctic climate. Some studies have emphasized the role of local feedbacks over the Arctic, which may enhance or diminish an initial temperature response; these include temperature feedbacks (Winton 2006, Pithan and Mauritsen 2014, Stuecker *et al* 2018), the surface albedo feedback (Holland and Bitz 2003, Screen and Simmonds 2010, Dai 2021), and cloud feedbacks (Vavrus *et al* 2011, Cao *et al* 2017, Jenkins and Dai 2022). Others attribute AA mainly to changes in heat transport into the Arctic by the atmosphere, specifically through enhanced moisture transport (Lee 2014, Merlis and Henry 2018, Graversen and Langen 2019, Russotto and Biasutti 2020) and the ocean (Bitz *et al* 2006, Singh *et al* 2017, van der Linden *et al* 2019). This issue is further complicated by the coupling between different local feedbacks or energy transports, which may obscure the effect of individual contributions to AA (Hwang *et al* 2011, Graversen *et al* 2014, Feldl *et al* 2017, Chung *et al* 2021, Previdi *et al* 2021). For example, although the lapse rate (LR) feedback, a type of temperature feedback, is often considered in isolation, it is strongly linked to sea ice loss, atmospheric heat transport (AHT), and surface temperature response (Feldl *et al* 2020, Boeke *et al* 2021).

It is important to note that these proposed AA mechanisms operate on different timescales, mainly because of the different rates with which climate system components respond to radiative forcing (RF). However, most previous studies of AA do not discriminate between these different timescales and focus on the long-term (e.g., multi-decadal) or equilibrium response to an imposed forcing. An exception to this is the recent study of Previdi *et al* (2020), which focused specifically on the different timescales of AA. In that study, a collection of models from the Coupled Model Intercomparison Project Phase 5 (CMIP5) subjected to an instantaneous quadrupling of CO₂ relative to preindustrial levels was analyzed, and the contributions of different AA mechanisms were quantified. It was shown that the relative importance of various mechanisms depends on the timescale; for example, the LR feedback is the main contributor to AA across CMIP5 models in the first three months following the CO₂-quadrupling, but in the last 30 years of the simulations (representing the quasi-equilibrium response), the surface albedo feedback dominates (Previdi *et al* 2020). Thus, to elucidate the relative contributions of different mechanisms to AA, one must pay careful attention to the timescale being considered. The main conclusion of Previdi *et al* (2020) is that AA is inherently a rapid response to RF, fundamentally owing its existence to fast atmospheric processes.

Although an important first step, the study by Previdi *et al* (2020) was hampered by several factors. First, only 21 CMIP5 models provided the variables necessary to complete an energy budget analysis. This relatively small sample size made it difficult to robustly characterize the evolution of AA, particularly on the short timescales of interest where internal variability (especially in the Arctic) is large. Second, CMIP5 output was only available as monthly means. This precluded any assessment of the role of sub-monthly processes in AA. Given the rapid timescale associated with AA, the coarse time resolution of the data and the lack of multiple realizations posed a key limitation to their conclusions based on CMIP5 data. Finally, all simulations analyzed in that study had CO₂ quadrupling on 1 January, leaving open the question of how the time evolution of AA would differ if CO₂ were quadrupled in different seasons. Bintanja and Krikken (2016) previously explored the impact of the season of CO₂ forcing on Arctic warming but at timescales beyond the initial response. The timing of CO₂ increase is particularly important in the Arctic, which cycles through 6 month polar days and nights, experiencing a very large seasonal cycle.

Here, we seek to overcome these limitations and build upon the work of Previdi *et al* (2020) by analyzing the development of AA using high-frequency (daily) output from climate model simulations subjected to an instantaneous quadrupling of CO₂. To address the small signal-to-noise ratio of the Arctic (Screen *et al* 2014, Swart *et al* 2015, England *et al* 2019), we generate two large ensembles of simulations (50–100 members) in which CO₂ is increased at different times during the year (either January or July). The questions we seek to answer are as follows:

- How quickly does AA develop in an ensemble of model simulations subjected to an instantaneous CO₂ increase?
- What mechanisms best explain the initial appearance and the subsequent evolution of AA?
- How does the time of year in which atmospheric CO₂ is quadrupled affect AA development?

2. Methods

2.1. Model description

In this study, we used the Community Earth System Model version 1, Large Ensemble configuration (CESM-LE). CESM-LE is a fully coupled global climate model (GCM) based on version 1.1.1 of the Community Earth System Model (CESM), a model included in CMIP5, and has active atmosphere, land, ocean, and sea ice components. The atmosphere model in CESM-LE is the Community Atmosphere Model

version 5 (CAM5), with a horizontal resolution of $\sim 1^\circ$. For more detailed information about the CESM-LE configuration, see Kay *et al* (2015); for CAM5, see Hurrell *et al* (2013).

CESM-LE is well-suited for studies of Arctic climate because of its ability to simulate the modern Arctic sea ice state (Jahn *et al* 2016) and its outperformance of other CMIP5 models in capturing the internal variability of Arctic sea ice (England *et al* 2019). Consequently, CESM-LE has a strong precedent of use in Arctic climate studies (e.g., Jahn *et al* 2016, Labe *et al* 2018, Yang and Magnusdottir 2018).

2.2. Experiment design

We generated large ensembles of simulations with CESM-LE, with individual ensemble members differing only in their initial conditions. The initial conditions were chosen randomly from an existing ~ 2200 year-long CESM-LE control simulation with fixed preindustrial forcing available on National Center for Atmospheric Research machines (Kay and Deser 2016). This initialization approach was chosen to better sample climate state variability in the days following CO_2 increase by ensuring that ensemble realizations are sufficiently different, as opposed to the method used in Kay *et al* (2015), in which small round-off level perturbations are introduced to initial conditions. The existing control simulation had restart files available every ~ 5 years. Our ensembles consist of paired 2 year-long CESM-LE runs. The first run in each pair has fixed preindustrial forcing (piControl), while the second is subjected to an instantaneous CO_2 -quadrupling relative to preindustrial levels ($4 \times \text{CO}_2$).

To investigate the impact of the time of year of $4 \times \text{CO}_2$ on AA, we created two ensembles, one containing members initialized on 1 January and the other with members initialized on 1 July of the same model year. Because restart files from the existing CESM-LE run were only available for 1 January, we generated new restart files for July from our January-initialized piControl simulations. All model output was saved as daily averages.

For the sake of readability, we henceforth refer to the experiment in which CO_2 is quadrupled in January as Jan $4 \times \text{CO}_2$ and in July as Jul $4 \times \text{CO}_2$. Jan $4 \times \text{CO}_2$ and Jul $4 \times \text{CO}_2$ have 100 and 50 ensemble members, respectively. These ensemble sizes were determined carefully considering the seasonality of Arctic internal variability and computational constraints, along with the suggestion of a 100-member minimum in the Polar Amplification Model Intercomparison Project (Smith *et al* 2019). Given the large internal variability in the Arctic region, we ran multiple members to ensure that a forced AA signal could be separated from the variability; we later show results with different ensemble sizes for context.

2.3. Energy budget analysis

2.3.1. Framework

We compare the global average and Arctic energy budgets to understand how the CO_2 RF, climate feedbacks, and energy transports contribute to AA. We define the Arctic as the region from 70°N to 90°N , with approximately the same fractional land area as the global average (~ 0.29). Because of the fast timescales in our analysis, we prefer not to use the ratio of Arctic to global warming to avoid dividing by near-zero global temperature changes. Therefore, we generally define AA and warming contributions to AA as the difference between the Arctic and global averages.

We adopt an energy budget framework similar to that of Pithan and Mauritsen (2014), Goosse *et al* (2018), Zhang *et al* (2018), and Previdi *et al* (2020). We consider an atmospheric column that extends from the top of the atmosphere (TOA) to the surface, with R representing the net downward radiative flux at the TOA. If we introduce a TOA radiative imbalance by subjecting the column to some RF ΔF , we can relate the imbalance and forcing as follows:

$$\Delta R = \Delta F + \lambda \Delta T_s + \Delta AHT + \Delta SHU \quad (1)$$

where λ is the local climate feedback parameter, T_s is the surface air temperature, AHT is the vertically integrated convergence of the atmospheric heat transport, and SHU is the surface heat uptake, defined as positive upwards (i.e., into the column). Δ represents the difference between the piControl and $4 \times \text{CO}_2$ simulations. Because of the short timescales of interest, we take ΔF to be the instantaneous RF at the TOA from $4 \times \text{CO}_2$. We compute this RF using the Parallel Offline Radiative Transfer (PORT) model with CESM (Conley *et al* 2013). Responses to the instantaneous CO_2 forcing that affect ΔR and ΔSHU are generally referred to as ‘feedbacks’ for ease of discussion. However, in section 6, we consider which of these responses may be more appropriately regarded as ‘rapid adjustments.’

We decompose the net climate feedback parameter λ as follows (Pithan and Mauritsen 2014, Goosse *et al* 2018, Zhang *et al* 2018):

$$\lambda = \lambda_o + \sum_x \lambda_x \quad (2)$$

where λ_0 is the Planck feedback, and λ_x represents feedbacks due to changes in water vapor, clouds, the atmospheric LR, and surface albedo. Following past studies (Pithan and Mauritsen 2014, Goosse *et al* 2018), we further decompose the Planck feedback into a global mean value $\overline{\lambda_0}$ and local deviation from the global mean, λ_0' :

$$\lambda_0 = \overline{\lambda_0} + \lambda_0'. \quad (3)$$

The AHT into the Arctic is computed directly from model covariance fields. The meridional flux of moist static energy into the Arctic can be written as follows:

$$AHT = \frac{C}{2\pi A} \int_0^{2\pi} \int_0^{p_s} \frac{\nu (c_p T + gz + L_v q) dx dp}{g} \quad (4)$$

with A being the area of the Arctic, C the circumference of the southern latitudinal boundary of the Arctic, p_s the surface pressure, ν the meridional component of the wind, c_p the specific heat of dry air, T the air temperature, g the gravitational constant, L_v the latent heat of vaporization of water, and q the specific humidity (Cardinale *et al* 2021). The global average AHT convergence is zero, by definition.

Because covariance terms involving the zonal component of the wind were not available, we calculate the AHT convergence as a residual when estimating warming contributions separately for land and ocean (see section 5):

$$AHT = \frac{dE}{dt} - SHU - R \quad (5)$$

where $\frac{dE}{dt}$ is the time rate of change in atmospheric column energy, SHU is the surface heat uptake, and R is the net radiative flux at the TOA, as in equation (1). The AHT calculated as a residual closely matches the direct calculation (not shown).

The SHU is equal to the net surface heat flux from the model. It can be decomposed into radiative and non-radiative components; the former includes contributions from surface RF and feedbacks, and the latter contains sensible and latent heat fluxes:

$$\Delta SHU = \Delta F_{sfc} = \Delta F_{CO_2} + \Delta F_{LH} + \Delta F_{SH} + \Delta T_s \sum_x \lambda_{s,x} \quad (6)$$

F_{sfc} is the net surface heat flux, ΔF_{CO_2} is the instantaneous $4 \times CO_2$ RF from CESM-PORT at the surface, F_{LH} is the latent heat flux, F_{SH} is the sensible heat flux, and $\lambda_{s,x}$ represents feedbacks at the surface from changes in temperature, water vapor, clouds, and surface albedo. The radiative feedbacks at the surface are mostly analogous to their TOA counterparts in that they quantify radiative perturbations from changes in certain fields at the surface instead of the TOA. As in equation (1), SHU and all of its components are defined such that positive values indicate the flow of energy from the surface into the atmospheric column. This sign convention at the surface is opposite to that of Pithan and Mauritsen (2014) and Láiné *et al* (2016). We offer two reasons for this difference. First, SHU should be positive and, therefore, contribute to Arctic warming in the fall and winter, when the ocean acts as a heat source to the atmosphere (Screen and Simmonds 2010, Bintanja and van der Linden 2013, Boeke and Taylor 2018, Chung *et al* 2021, Dai *et al* 2021). Second, on the longer, annual timescales analyzed by Pithan and Mauritsen (2014) and Láiné *et al* (2016), energy added to the surface is ultimately realized as surface warming; this is not necessarily true on the fast timescales examined in this study for which we must account for the storage of heat in the surface.

2.3.2. Feedback calculations

We use the radiative kernel technique to quantify the radiative perturbations at the TOA and surface from climate feedbacks (Shell *et al* 2008, Soden *et al* 2008). We employ the CAM5 kernels documented in Pendergrass *et al* (2018), which have the same horizontal resolution and underlying radiation code as our CESM-LE simulations and were created with CESM 1.1.2 fields (e.g., temperature, moisture, and clouds). The kernels were only available as monthly averages, so they were linearly interpolated with periodic boundary conditions to a daily resolution to match the model output. Height-dependent kernels and model output were linearly regridded from the native hybrid-sigma coordinates to standard pressure levels for feedback calculations.

The TOA temperature feedback was separated into Planck and LR components. For the Planck feedback, a vertically uniform temperature change equal to the surface air temperature change was assumed. The LR feedback was calculated as the departure from this vertically uniform temperature change. We used the change in the natural logarithm of the specific humidity to compute the radiative perturbation due to water vapor feedback (Soden *et al* 2008). Tropospheric temperature and water vapor feedbacks are vertically

integrated from the surface to the model-defined tropopause. Stratospheric feedbacks are quantified similarly by integrating from the tropopause to the TOA.

The temperature feedback at the surface was decomposed into surface warming and atmospheric warming feedbacks, corresponding to changes in outgoing longwave radiation (OLR) from the surface and incoming longwave radiation from the atmosphere received by the surface, respectively (Pithan and Mauritsen 2014).

The cloud feedback (ΔR_{cloud}) is determined using the ‘adjustment method’ developed by Soden *et al* (2008). In this method, the change in cloud radiative effect (ΔCRE) is adjusted to remove the effects of cloud masking, i.e.:

$$\Delta R_{\text{cloud}} = \Delta \text{CRE} - (\Delta F - \Delta F^o) - \sum_x (\Delta R_x - \Delta R_x^o) \quad (7)$$

where ΔF and ΔR_x represent the all-sky radiative perturbations at the TOA or surface due to climate forcing and feedbacks, respectively, and the superscript o indicates the clear-sky perturbations (e.g., see Zhang *et al* 2018).

We express forcing, feedback, and transport terms as warming contributions to the global or Arctic average surface air temperature response, as was done by Crook *et al* (2011), Feldl and Roe (2013), Pithan and Mauritsen (2014), Goosse *et al* (2018), and Previdi *et al* (2020). This is achieved by normalizing each term (in W m^{-2}) by the magnitude of the time-averaged ensemble-mean global Planck feedback ($\sim 3.2 \text{ W m}^{-2} \text{ K}^{-1}$). For the code used to perform all calculations, see Janoski (2023).

3. Rapid AA after $4 \times \text{CO}_2$

We begin by observing the evolution of the global and Arctic average surface air temperature (SAT) response in Jan $4 \times \text{CO}_2$ (figure 1(a)). AA rapidly develops as the ensemble mean Arctic SAT response quickly diverges from the global average within days after $4 \times \text{CO}_2$. In the first week, the ensemble mean Arctic warming is nearly double that of the global average (0.75 K vs. 0.34 K); this difference grows when the first three months are considered (1.69 K vs. 0.68 K), comparable to the Arctic-to-global warming ratio reported in Previdi *et al* (2020) over the same timescale. In Jul $4 \times \text{CO}_2$ (figure 1(b)), it takes longer for the Arctic and global average temperature responses to diverge, corresponding to the well-observed seasonally reduced AA in boreal summer (Lainé *et al* 2016). Even with the slower start in Jul $4 \times \text{CO}_2$, the Arctic warms considerably more than the global average in the first three months (1.52 K vs. 0.82 K). The pronounced seasonal variability in Arctic SAT response is the most prominent feature in the later periods of the simulations.

To determine statistical significance, we perform a 1-sample Student’s t-test on the time series of AA, shown in figures 1(c) and (d). In the Jan $4 \times \text{CO}_2$, AA is statistically significant from day one and remains significant for almost the entire 2 year period, owing to the large ensemble size. In Jul $4 \times \text{CO}_2$, AA becomes consistently significant after 25 d and remains so, aside from 2 weeks in the first March. AA, therefore, can be detected well before the first three months following CO_2 -quadrupling seen in Previdi *et al* (2020), given sufficient ensemble size and temporal resolution. Until now, these ultrafast timescales of AA have been relatively unexplored in the existing body of AA research.

We note that the general features of the SAT and AA responses seen in figure 1 are robust to the number of ensemble members considered, although, not surprisingly, the responses are noisier and less statistically significant for smaller ensemble sizes (figures S1 and S2). The considerable noise in the Arctic SAT response (red lines) in figures S1(a), (c) & (e) and of figures S2(a) & (c) reflect the large internal variability present in the Arctic and the need for sufficiently large ensemble sizes in studies of Arctic climate.

Given the prominent role sea ice loss is thought to play in AA, we next explore how sea ice area (SIA) evolves over the same timescales. Sea ice loss is negligible in the first month of Jan $4 \times \text{CO}_2$ and remains relatively small through the rest of the winter and early spring (figures 2(a) and (c)), suggesting that sea ice loss plays a minimal role in AA on these short timescales. The decline in SIA accelerates through the late spring and summer, culminating in a $\sim 30\%$ decrease by the first September in Jan $4 \times \text{CO}_2$. The minimum in SIA precedes the seasonal AA maximum in Jan $4 \times \text{CO}_2$ by 1–2 months (figure 1(c)), implying a large role for sea ice loss in governing the seasonality of AA through its effects on ocean-atmosphere heat exchange (see additional discussion in section 4.2).

Sea ice loss exhibits a considerably different temporal structure in Jul $4 \times \text{CO}_2$ (figures 2(b) and (d)). We see a rapid decline in SIA over the first two months ($\sim 9\%$ decrease by September), which then plateaus and slightly reverses through the following fall, winter, and spring. Interestingly, despite the immediate SIA reduction in Jul $4 \times \text{CO}_2$, AA is larger and more robust in the first month of Jan $4 \times \text{CO}_2$ with negligible sea ice loss. We discuss spatial changes in sea ice and their relationship with the surface air temperature response in section 5.

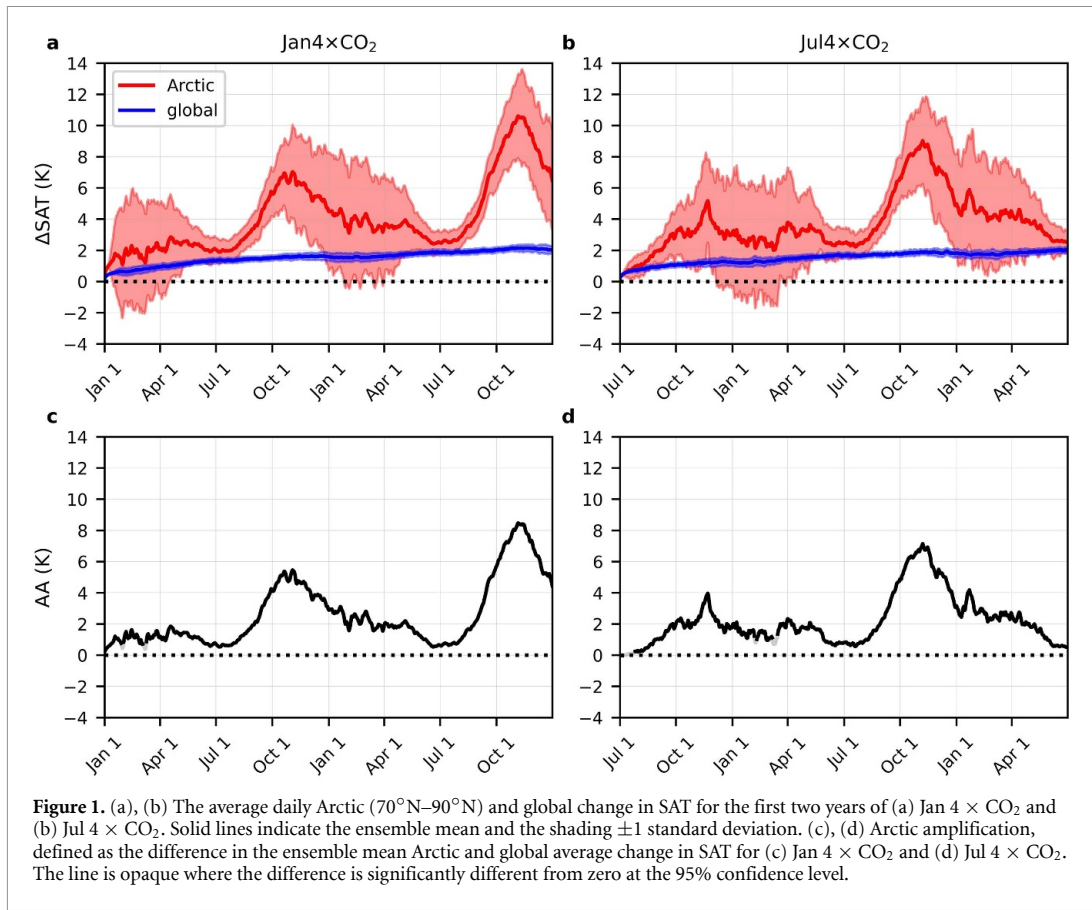


Figure 1. (a), (b) The average daily Arctic (70°N–90°N) and global change in SAT for the first two years of (a) Jan 4 × CO₂ and (b) Jul 4 × CO₂. Solid lines indicate the ensemble mean and the shading ±1 standard deviation. (c), (d) Arctic amplification, defined as the difference in the ensemble mean Arctic and global average change in SAT for (c) Jan 4 × CO₂ and (d) Jul 4 × CO₂. The line is opaque where the difference is significantly different from zero at the 95% confidence level.

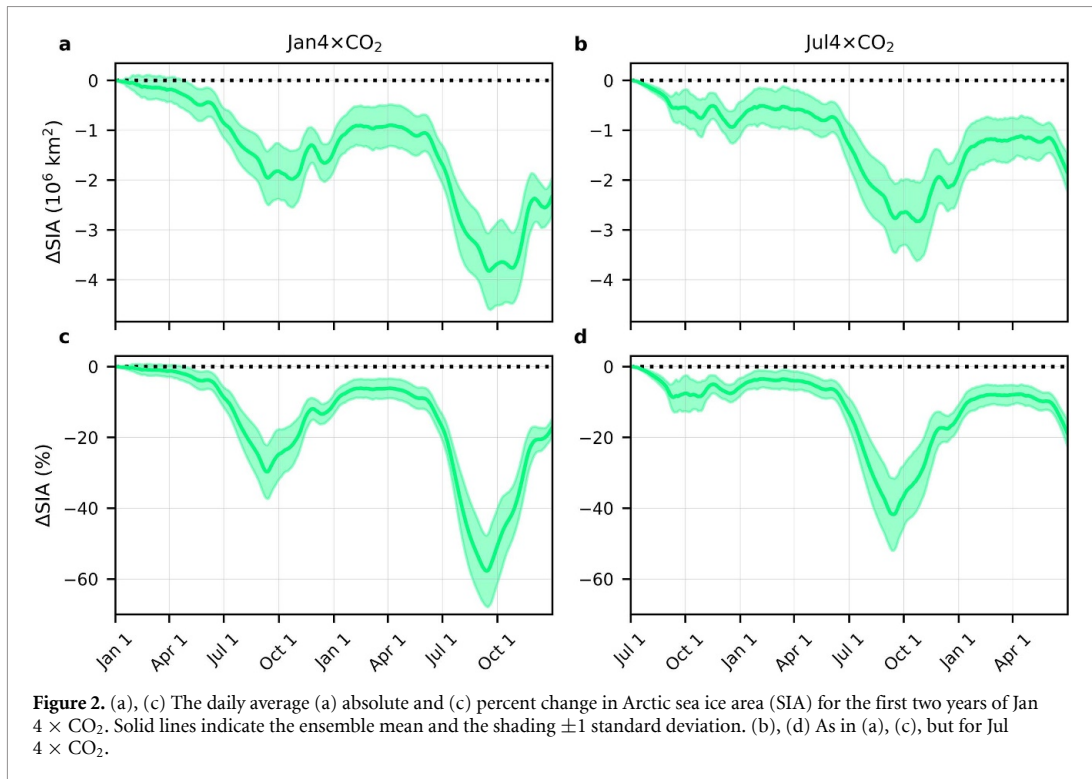
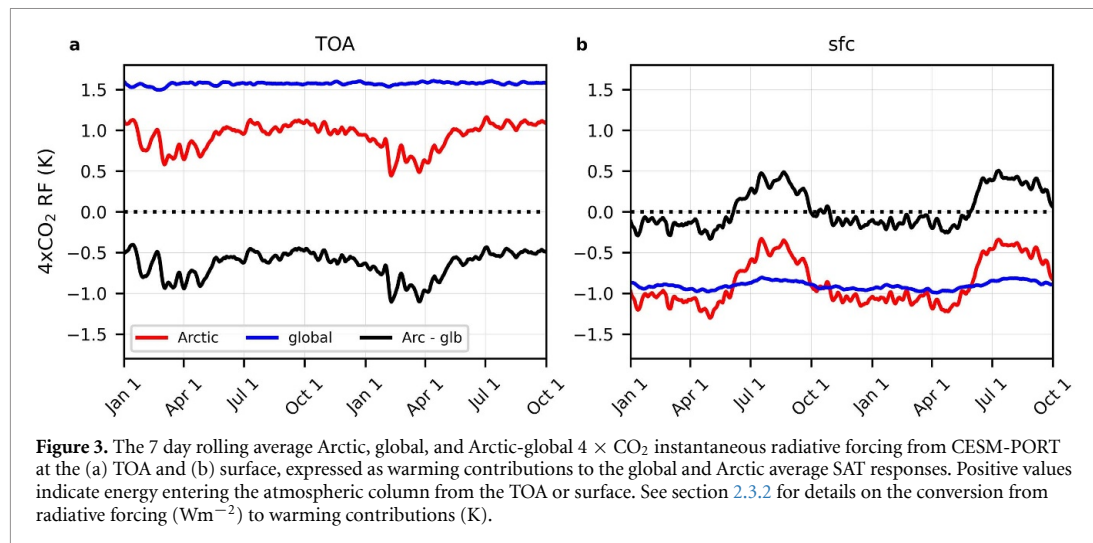


Figure 2. (a), (c) The daily average (a) absolute and (c) percent change in Arctic sea ice area (SIA) for the first two years of Jan 4 × CO₂. Solid lines indicate the ensemble mean and the shading ±1 standard deviation. (b), (d) As in (a), (c), but for Jul 4 × CO₂.



4. Mechanism contributions to AA

4.1. Radiative forcing

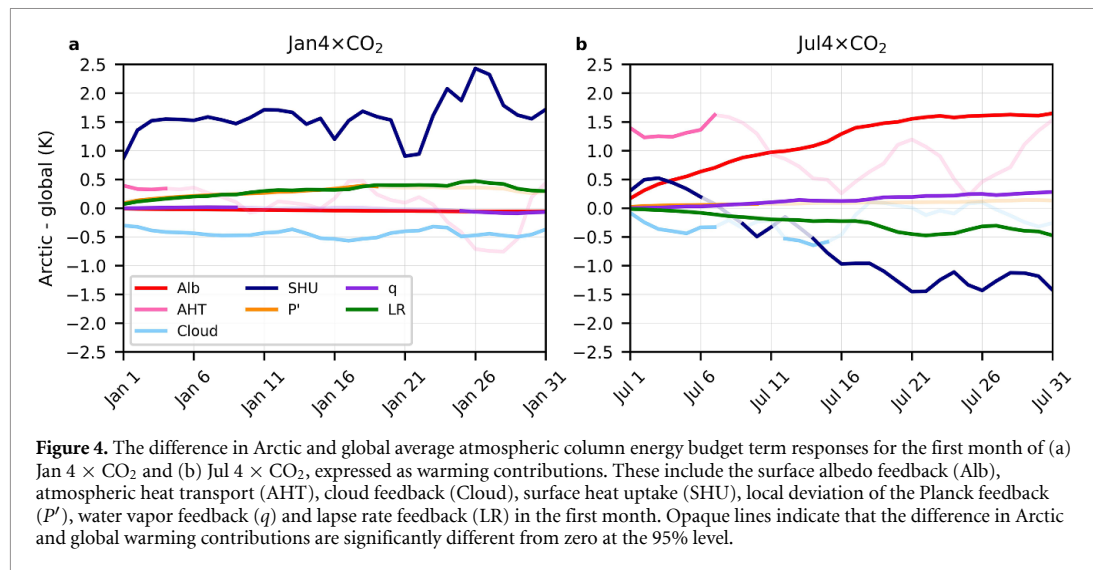
Having shown that AA becomes statistically significant almost immediately in Jan $4 \times \text{CO}_2$ and in the first month of Jul $4 \times \text{CO}_2$, we now quantify the time-varying warming contributions of different AA mechanisms. A natural place to start is the fundamental driver of the climate response, the RF associated with $4 \times \text{CO}_2$ (figure 3). The magnitude of the $4 \times \text{CO}_2$ RF at the TOA (figure 3(a)) is mainly determined by two factors: the climatological surface temperature and the temperature LR. The climatological surface temperature governs the RF via the Stefan–Boltzmann law: warmer surfaces produce more OLR for CO_2 to absorb and re-emit into the atmospheric column (Raval and Ramanathan 1989; Huang *et al* 2016a). The LR determines the temperature of the atmospheric layer from which OLR is effectively emitted to space; increased CO_2 can be thought of as increasing the height of this layer or, equivalently, decreasing the effective emission temperature, making the LR a pivotal factor in determining the TOA RF (Raval and Ramanathan 1989, Huang *et al* 2016a). The higher climatological surface temperature and larger temperature difference between the surface and upper troposphere in the global mean than in the Arctic yield a larger global mean TOA RF than Arctic mean TOA RF. Thus, when viewed from a TOA perspective, the CO_2 RF opposes AA.

A different story emerges when we consider the $4 \times \text{CO}_2$ RF at the surface (figure 3(b)), which is strongly affected by the overlap in the spectral bands of CO_2 and water vapor (Kiehl and Ramanathan 1982, Huang *et al* 2017, Previdi *et al* 2021). The forcing is consistently negative for both the Arctic and global average, indicating that the surface is gaining energy from the atmosphere. From October to April, the Arctic surface intercepts slightly more energy than the global average, opposing AA; this reverses in the summer.

Although we have treated the CO_2 RF as a standalone AA mechanism in the spirit of separating the forcing from the climate system response, we remind the reader that the surface CO_2 RF is incorporated into the SHU term (see equation (6)). The contribution from the surface CO_2 RF to AA is small compared to the other terms in the surface energy budget that are discussed in section 4.3.

4.2. Atmospheric column energy budget

Having examined the CO_2 forcing, we move on to feedbacks and energy transports from an atmospheric column perspective. We start by focusing exclusively on the first month following $4 \times \text{CO}_2$ (figure 4). In Jan $4 \times \text{CO}_2$ (figure 4(a)), two mechanisms stand out as main AA contributors: the SHU, to be discussed in more detail later, and the LR feedback. It is worth mentioning how the LR feedback is thought to operate. Globally, the rate of temperature decrease with height in the troposphere is expected to decrease with increasing CO_2 —associated with enhanced warming at higher levels in the tropical troposphere—yielding a negative LR feedback. In the Arctic, however, the climatologically stable temperature stratification of the lower troposphere traps warming near the surface and produces a positive LR feedback (Graversen *et al* 2014, Pithan and Mauritsen 2014, Previdi *et al* 2021). In the first month of Jan $4 \times \text{CO}_2$, the SHU and LR feedback warm the Arctic up to 2.5 K and 0.4 K more than the global average, respectively, and are both statistically significant. Therefore, the rapid development of AA on short timescales in Jan $4 \times \text{CO}_2$ appears mainly to be a result of these two mechanisms. Previdi *et al* (2020) found that the LR feedback is a primary mechanism of AA on short timescales, and our results here support this. Other notable features in figure 4(a) are the Planck



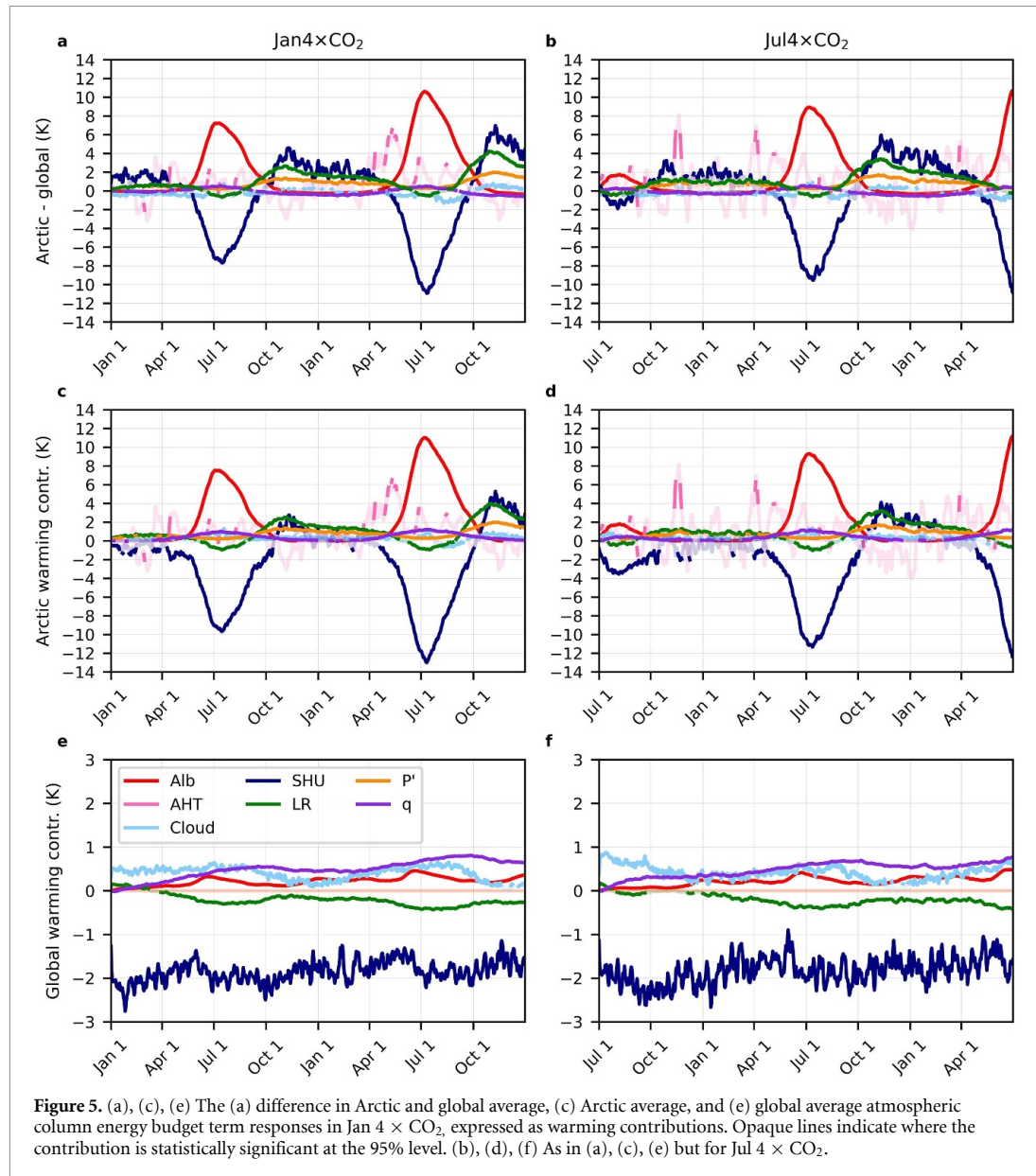
feedback that significantly contributes to AA only for the first few weeks and the cloud feedback that opposes AA throughout the first month in our model.

For Jul $4 \times \text{CO}_2$ (figure 4(b)), we find an initially positive AA contribution from SHU, but it becomes negligible and reverses (to oppose AA) within the first week. Instead, the AHT is the leading AA mechanism for the first week before becoming statistically nonsignificant and being surpassed by the surface albedo feedback. The surface albedo feedback remains the dominant AA-producing mechanism for the first month and is related to the rapid decline in sea ice seen in figures 2(b) and (d) and reductions in snow cover. Additionally, the water vapor feedback contributes to AA, albeit weakly.

On timescales beyond the first month, other mechanisms become important in shaping the magnitude and seasonality of AA. As seen in figures 5(a) and (b), the most striking features of the time-varying warming contributions to AA for both Jan $4 \times \text{CO}_2$ and Jul $4 \times \text{CO}_2$ (figures 5(a) and (b)) are the opposing peaks in the surface albedo feedback and SHU in boreal summer. The surface albedo feedback has typically been thought to be a major player in AA (Holland and Bitz 2003, Winton 2006, Bintanja and van der Linden 2013, Dai 2021); however, its seasonality does not match the seasonality of AA (see figures 1(c) and (d)), suggesting that other mechanisms must act to delay or modify its impacts. The opposing peaks in the surface albedo feedback and SHU in the summer supports the idea that as sea ice melts, incoming solar radiation that would otherwise have been reflected out to space is absorbed by the ocean surface. This additional heat absorbed by the ocean mixed layer is subsequently released to the atmosphere in fall and winter (e.g., Stroeve *et al* 2012, Boeke and Taylor 2018, Chung *et al* 2021, Hahn *et al* 2021, Jenkins and Dai 2022), thus contributing to the peak in AA in these seasons.

A few of the other terms in figure 5 are worth mentioning, notably the Planck feedback. The Planck feedback reflects a change in OLR in response to a given change in surface temperature, and its difference between the Arctic and global average is thought to be an important contributor to AA (Winton 2006, Pithan and Mauritsen 2014, Zhang *et al* 2018 Henry and Merlis 2019, Previdi *et al* 2020). Although the Planck feedback produces a small but statistically significant contribution to AA beginning in the first March of Jan $4 \times \text{CO}_2$ (figure 5(a)), only in the following winter does it become one of the main AA-producing mechanisms. The water vapor feedback also makes small contributions to AA in boreal summer in both Jan $4 \times \text{CO}_2$ and Jul $4 \times \text{CO}_2$ (figures 5(a) and (b)). The water vapor feedback's peak contribution in the summer may be related to increased moisture transport into the Arctic, discussed later. Lastly, the AHT is very noisy compared to the other terms and does not contribute robustly to AA (figures 5(a) and (b)).

Let us now investigate further into this statistically nonsignificant AHT. Despite the lack of discernable signal in the total AHT, it is possible that the dry static energy convergence (S_{conv}) and the moisture flux convergence (W_{conv}) into the Arctic, shown in figure 6, individually contribute to the development of AA (Held and Soden 2006). AA is generally associated with decreases in S_{conv} into the Arctic, resulting from the reduced latitudinal temperature gradient, and increases in W_{conv} into the Arctic, a product of the strengthening latitudinal specific humidity gradient (Hwang *et al* 2011, Graversen and Burtu 2016, Previdi *et al* 2021). In particular, W_{conv} has been suggested to be a main driver of AA in the context of simplified models (Russotto and Biasutti 2020). As we can see in figure 6, over the two years of our model simulations, S_{conv} is as noisy as the total AHT and does not consistently contribute to or oppose AA in either Jan $4 \times \text{CO}_2$

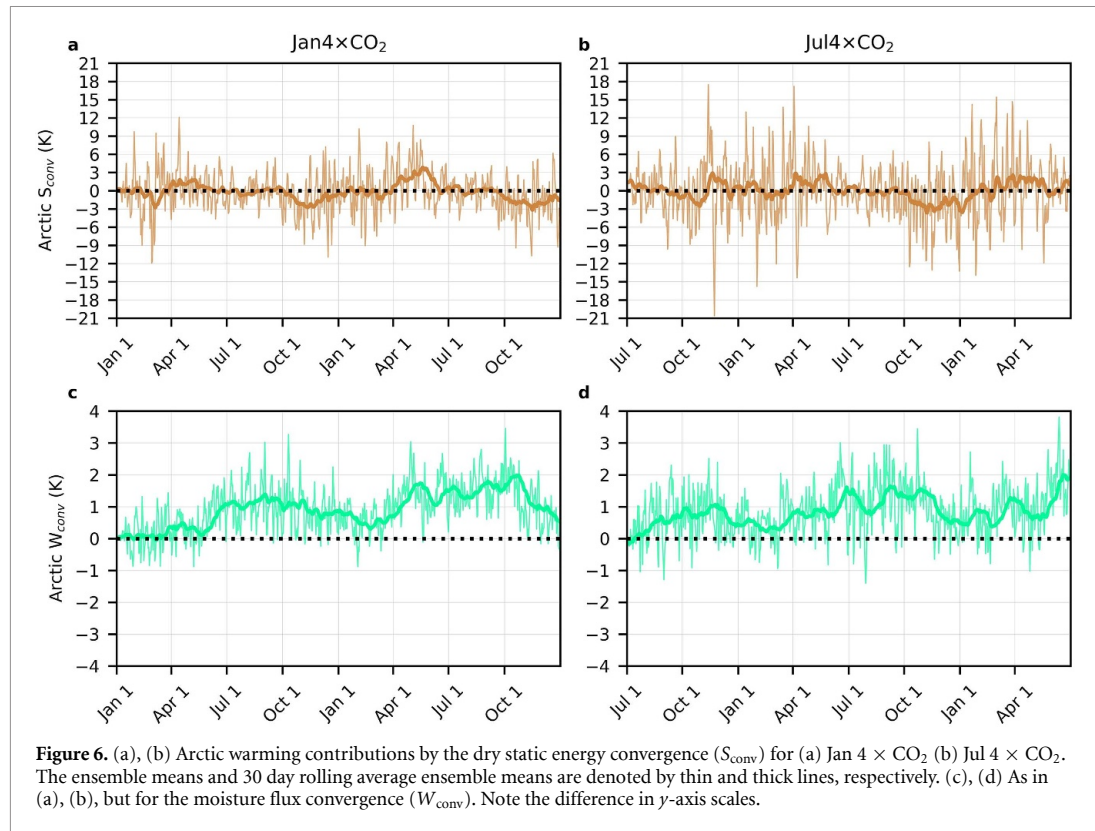


and $\text{Jul } 4 \times \text{CO}_2$ (figures 6(a) and (b)). W_{conv} contributes to AA mainly during boreal summer (figures 6(c) and (d)); this coincides with periods of positive contributions to AA from the water vapor feedback seen in figures 5(a) and (b). This suggests that W_{conv} affects the Arctic atmospheric energy budget both directly, and indirectly via the water vapor feedback (Gong *et al* 2017, Russotto and Biasutti 2020, Previdi *et al* 2021). However, we stress that the development of AA in $\text{Jan } 4 \times \text{CO}_2$ precedes any increase in the poleward moisture flux into the Arctic, meaning that the latter cannot explain the ultrafast development of AA following CO_2 increase.

Thus far in this section, we have considered only the tropospheric temperature and water vapor feedbacks. However, some studies have found that stratospheric feedbacks may play some role in the surface temperature response to increased CO_2 levels (Huang *et al* 2016b, Banerjee *et al* 2019). We have quantified the total temperature and water vapor feedbacks in the stratosphere (figure 7) and find that both are generally small contributions to AA compared to tropospheric feedbacks, aside from a brief period in the second spring of $\text{Jan } 4 \times \text{CO}_2$ in which the stratospheric temperature feedback contributes up to ~ 0.55 K to AA in the ensemble mean.

4.3. Surface energy budget

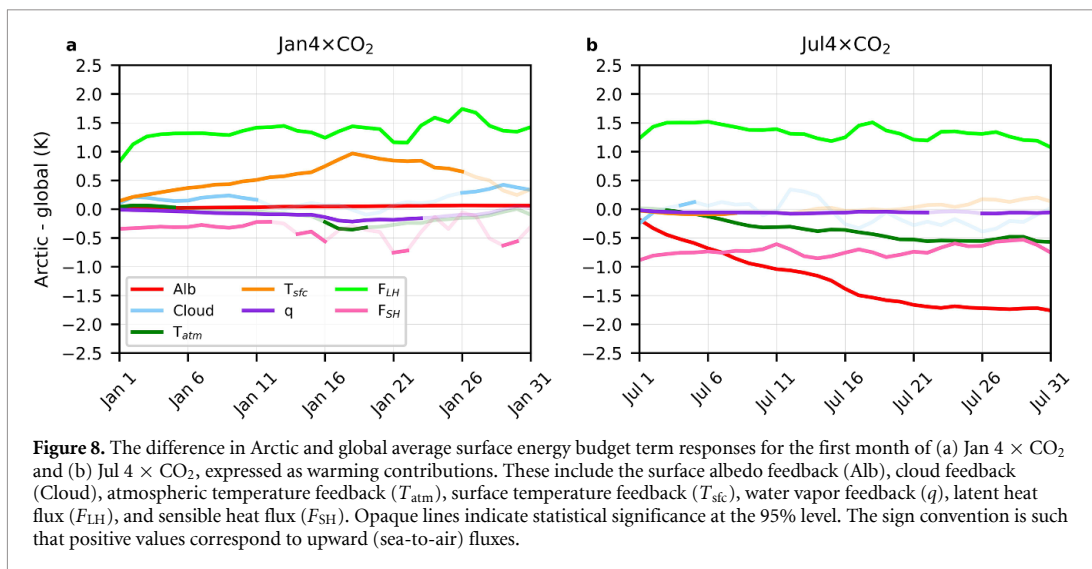
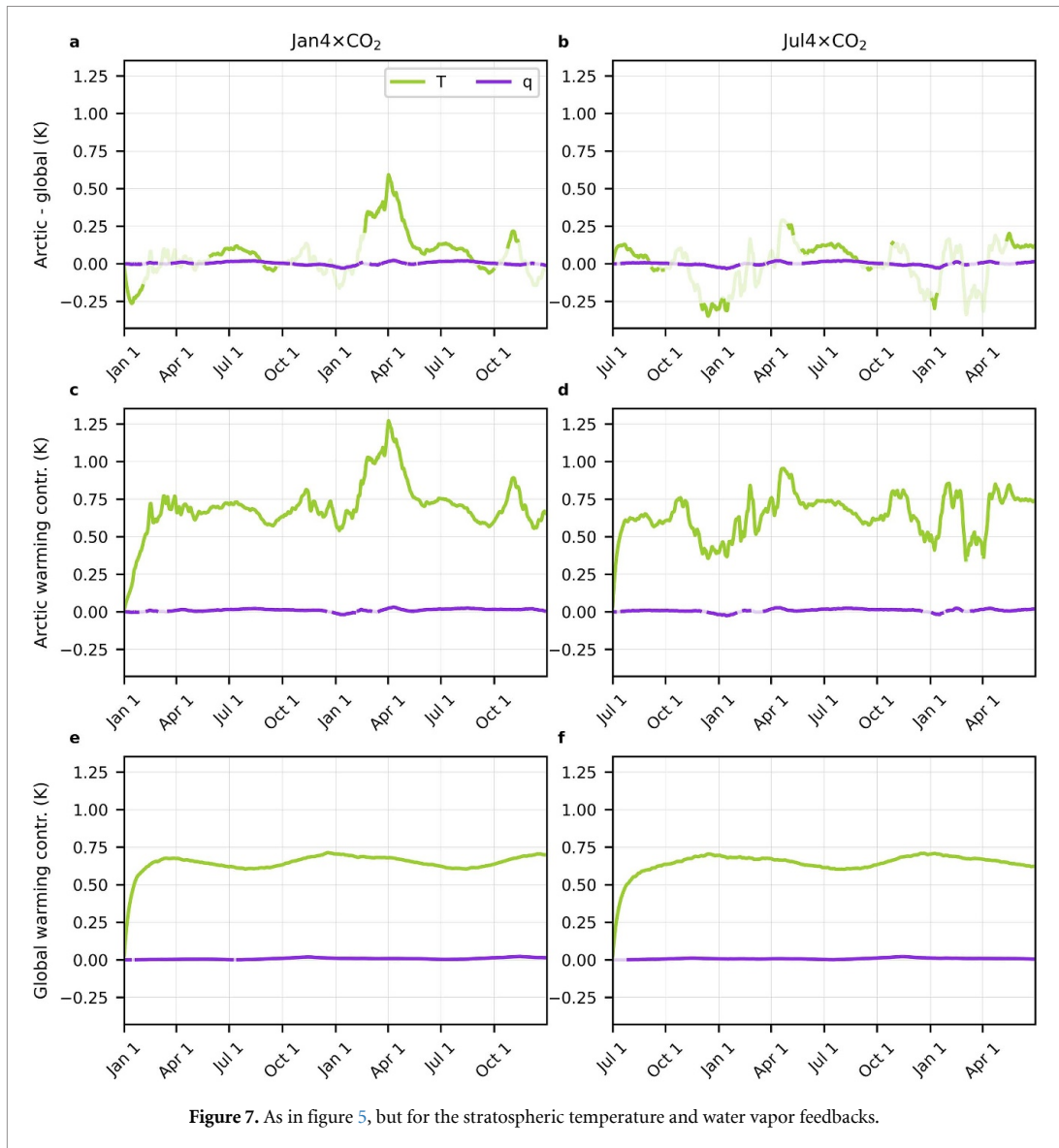
The bulk of our analysis so far has focused on the atmospheric column energy budget from a TOA perspective. Given the leading role of SHU in $\text{Jan } 4 \times \text{CO}_2$ in AA development (figure 4(a)) and the

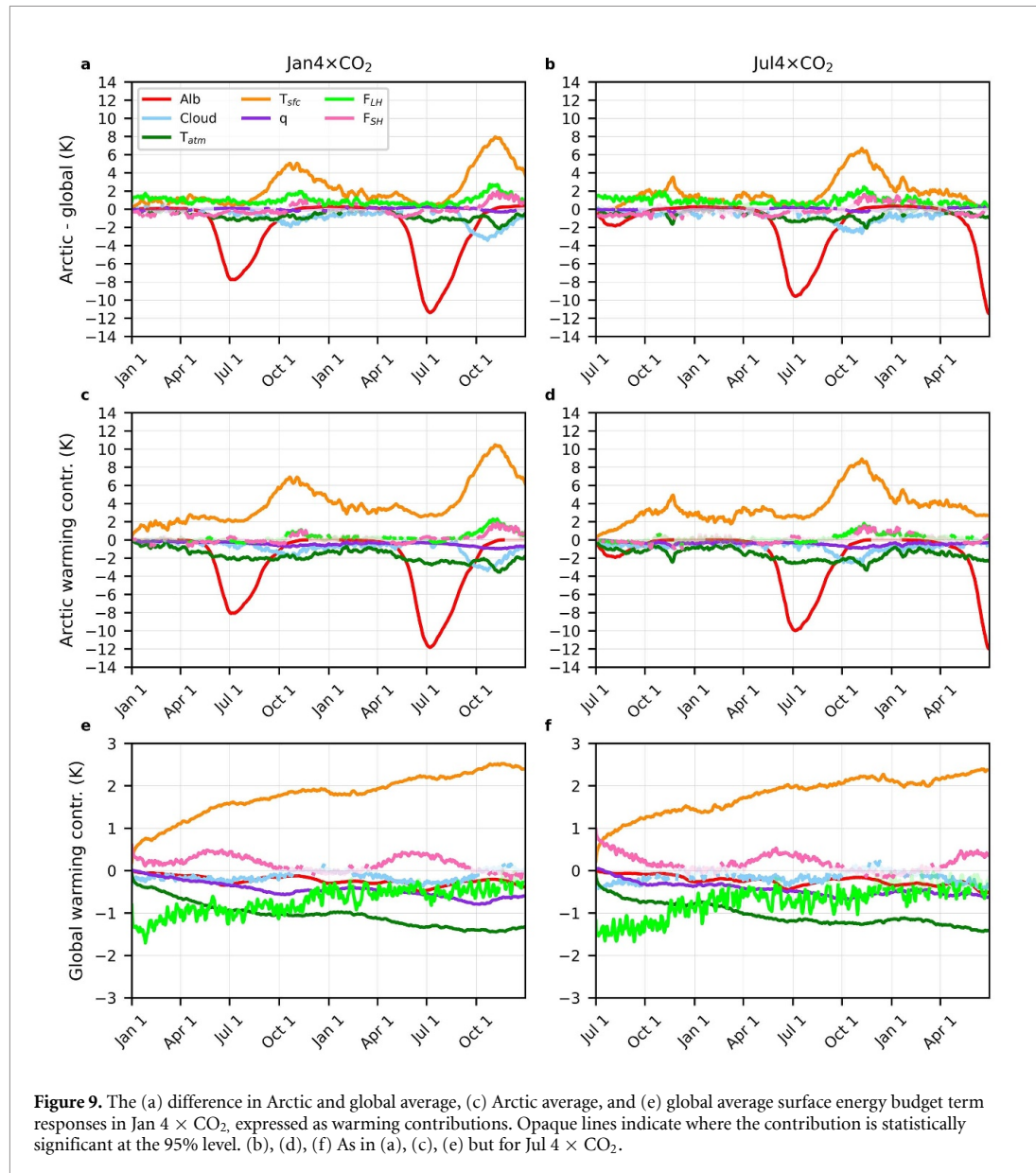


climatological stratification of the Arctic lower troposphere, we now take a closer look at the surface energy budget. We decompose the SHU response into contributions from radiative and non-radiative flux changes, which we show for the first month in figure 8, except for the CO_2 RF previously discussed in section 4.1. One of the more conspicuous features of the time-varying surface energy balance is the strong positive contribution to AA by the latent heat flux (F_{LH}) in both $Jan 4 \times CO_2$ and $Jul 4 \times CO_2$ (figures 8(a) and (b)). Over the first few days, F_{LH} cools the global average by ~ 1 K and ~ 1.4 K more than the Arctic in $Jan 4 \times CO_2$ and $Jul 4 \times CO_2$, respectively. The latent heat flux persists as the dominant AA mechanism at the surface for the remainder of the first month. In $Jan 4 \times CO_2$, AA is further reinforced by the surface temperature feedback (figure 8(a)). In $Jul 4 \times CO_2$, AA is opposed by negative contributions from the sensible heat flux (F_{SH}) and the surface albedo feedback (figure 8(b)). The magnitudes of other positive contribution terms are smaller than F_{LH} in the first month, supporting the latent heat flux's leading role at the surface in the ultrafast development of AA.

To determine if the latent heat flux stays the dominant term over longer timescales, we show the surface energy budget terms over the entire 2 year period in figure 9. The latent heat flux remains the largest positive contribution to AA in both $Jan 4 \times CO_2$ and $Jul 4 \times CO_2$, although the surface temperature feedback regularly surpasses it in the fall and winter as AA nears its peak (figures 9(a) and (b)); the strong positive surface temperature feedback in the Arctic (figures 9(c) and (d)) during these times reflects the large Arctic surface warming and associated enhancement of the surface upwelling LW radiation, a greater enhancement than occurs in the global average (figures 9(e) and (f)). Another prominent feature of the surface energy budget response is the recurring negative peaks in the surface albedo feedback in terms of both AA (figures 9(a) and (b)) and Arctic warming contributions (figures 9(c) and (d)). As previously stated, atmospheric warming from the surface albedo feedback in summer is not realized in that season, as the additional heat is absorbed by the ocean, producing these local minima in albedo warming contributions. Consistent with Boeke and Taylor (2018), small cold-season peaks in sensible and latent heat flux contributions to AA can be seen in $Jan 4 \times CO_2$ and in the second year of $Jul 4 \times CO_2$ as the energy stored in the ocean is released into the atmosphere.

The warming contribution of the surface latent heat flux to AA on short timescales (figures 8 and 9(a), (b)) warrants further discussion. It is well-established that rapid adjustments of the global hydrological cycle occur following a perturbation in atmospheric CO_2 . Specifically, because of the difference in CO_2 RF at the TOA and surface (figure 3), atmospheric radiative cooling decreases as CO_2 increases. This decrease in



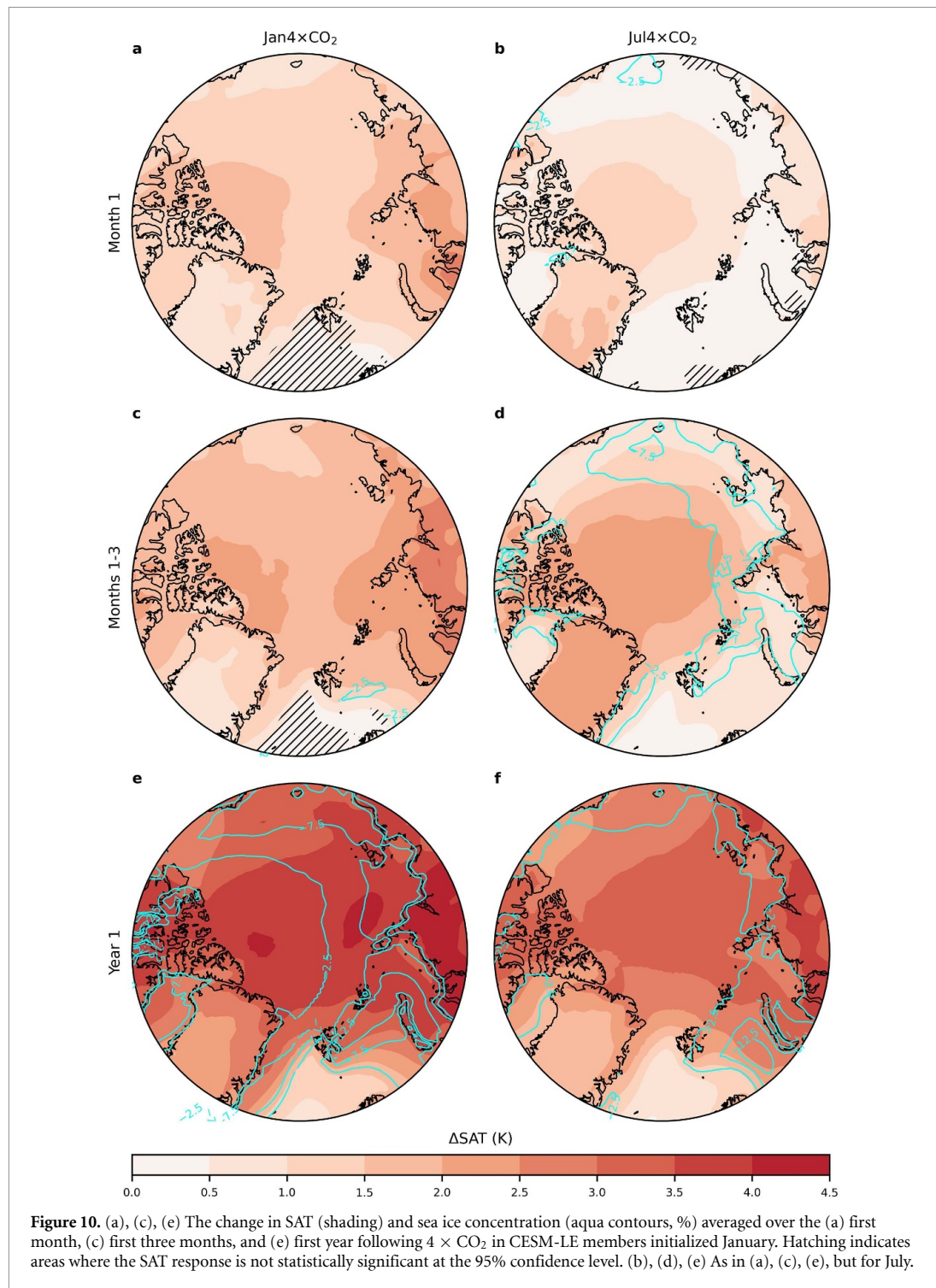


atmospheric radiative cooling must be balanced in the global mean by a decrease in latent heating from precipitation and, thus, a decrease in the upward surface latent heat flux (Allen and Ingram 2002, Bala *et al* 2010). This is reflected in the strong negative global F_{LH} anomaly occurring immediately after $4 \times \text{CO}_2$ in both Jan $4 \times \text{CO}_2$ and Jul $4 \times \text{CO}_2$ (figures 9(e) and (f)). Over the Arctic, any fast response of the surface F_{LH} is much smaller (figures 9(c) and (d)), resulting in a strong positive contribution from this term to AA.

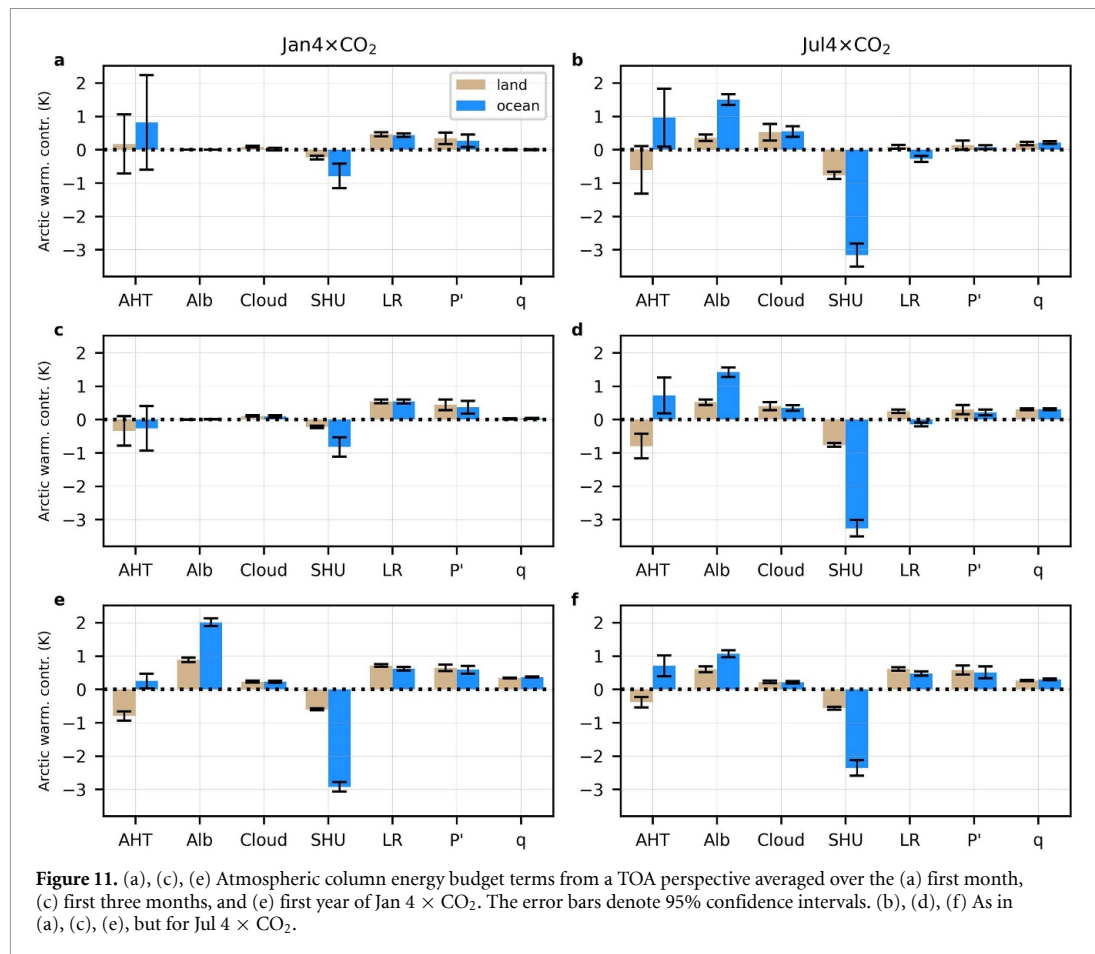
5. Arctic land vs. ocean response

Given the prominent role of SHU in AA development in Jan $4 \times \text{CO}_2$ and the potential role of sea ice, it is useful to consider the responses over Arctic land and ocean areas separately. We choose a few timescales over which to summarize the development of AA: the first month, the first three months, and the first year after $4 \times \text{CO}_2$. The first month roughly corresponds to the earliest timeframe in which AA is statistically significant in both the January- and July-initialized simulations, the first three months correspond to the earliest timescale analyzed in Previdi *et al* (2020), and the first year captures the first complete annual cycle following $4 \times \text{CO}_2$.

The spatial distribution of warming and its relationship to changes in Arctic sea ice for these periods is shown in figure 10. In the first month of Jan $4 \times \text{CO}_2$, there is statistically significant warming over the entire



Arctic domain except the Nordic Seas, with a local maximum in northern Siberia (figure 10(a)). Warming strengthens and spreads to include the entire domain over the first three months (figure 10(c)) and first year (figure 10(e)). Although $\text{Jul } 4 \times \text{CO}_2$ exhibits a greater decrease in sea ice in the first few months, the warming signal appears to be amplified over land rather than the ocean (figures 10(b) and (d)). By the end of the first year, $\text{Jan } 4 \times \text{CO}_2$ and $\text{Jul } 4 \times \text{CO}_2$ show similar spatial warming patterns, although overall warming is greater in $\text{Jan } 4 \times \text{CO}_2$ (figures 10(e) and (f)). By comparing the spatial distribution of SAT and SIC response on all three timescales, it is apparent that areas of maximum warming are *not* co-located with areas of maximum sea ice loss. This key result further demonstrates that mechanisms other than sea ice loss dominate the surface temperature response at these short timescales; however, we note that in the summer



sea ice melt season (figures 10(b) and (d)), Arctic SSTs are constrained to remain near the freezing point; thus, we expect greater warming over land where there is no such constraint.

To test the presence of land- or ocean-amplified warming, we show a time series of the SAT response averaged over Arctic land and ocean separately (figure S3). In both Jan $4 \times \text{CO}_2$ (figures S3(a) and (c)) and Jul $4 \times \text{CO}_2$ (figures S3(b) and (d)), a seasonal cycle emerges consisting of land-amplified warming in the summer and ocean-amplified warming in the fall and winter. Figures S3(d) confirms our suspicion from figures 10(b) and (d) that there is statistically significant land-amplified warming over the first few months of Jul $4 \times \text{CO}_2$.

To better understand the land and ocean SAT responses, we have calculated the warming contributions to the Arctic atmospheric column from a TOA perspective for the three time periods, for the land and ocean separately (figure 11). As one might expect, SHU is the term with the largest land–ocean difference over all periods in both Jan $4 \times \text{CO}_2$ and Jul $4 \times \text{CO}_2$, with the ensemble mean SHU response consistently at least three-times more negative over the ocean than over land. In Jan $4 \times \text{CO}_2$, this tendency for SHU to preferentially warm land is compensated by temperature feedbacks and AHT in the first few months (figures 11(a) and (c)), yielding little difference in the Arctic land and ocean temperature responses. The SHU is partially, but not fully, compensated by the surface albedo feedback on short timescales in Jul $4 \times \text{CO}_2$, producing the land-amplified warming seen in figures S3(b) and (d).

Given the magnitude of the SHU on short timescales relative to other terms in the TOA energy budget, we again decompose the SHU into individual terms in figure S4. As a reminder, the sign of the surface heat flux terms is chosen such that positive indicates the movement of energy from the surface to the atmospheric column. The sensible heat flux appears to be the main cause of land-over-ocean SHU warming in the first month and first three months of Jan $4 \times \text{CO}_2$ because it is positive over land and negative over the ocean (figures S4(a) and (c)). Over the first year of Jan $4 \times \text{CO}_2$ and all periods in Jul $4 \times \text{CO}_2$, the surface albedo feedback dominates land-over-ocean warming since it is considerably more negative for the ocean than land (figures S4(b), (d)–(f)). In other words, the surface albedo feedback moves a greater amount of energy from the atmospheric column into the ocean than into land. Thus, the surface albedo feedback and sensible heat

fluxes are the main drivers of the large contribution of SHU to the different Arctic land and ocean SAT responses.

6. Conclusions

In this study, we used two large ensembles of GCM simulations, one in which CO₂ is instantaneously quadrupled in January, the other in July, and observed how fast AA develops. We then attributed the AA response to local feedbacks and energy transports using an energy budget analysis from both TOA and surface perspectives. Finally, we analyzed the spatial pattern of Arctic warming and decomposed Arctic warming contributions into land and ocean components. Our results now allow us to revisit the key questions posed in the introduction:

How quickly does AA develop in an ensemble of model simulations subjected to an instantaneous CO₂ increase? Following a quadrupling of CO₂ in January or July, statistically significant AA develops in less than a month. In Jan 4 × CO₂, AA develops immediately (i.e., on day 1) after the RF is applied, whereas robust AA develops after 25 d in Jul 4 × CO₂.

To the best of our knowledge, our findings are novel in that AA has rarely been examined on such short timescales, with previous studies focusing on much longer (e.g., multi-decadal) timescales. An exception to this is the recent study by Previdi *et al* (2020). In that study, which used monthly mean model output, AA was present after three months following an abrupt quadrupling of CO₂ in January. Our use of large ensembles of daily output for the present study allowed AA to be detected considerably earlier with the same CO₂ forcing. Notably, AA precedes any statistically significant decrease in Arctic sea ice in January-initialized simulations; conversely, AA development tends to lag the response of the SIA in Jul 4 × CO₂. This demonstrates that the development of AA does not require a decrease in Arctic sea ice, confirming the findings of Previdi *et al* (2020) and supports the results of several other modeling studies that employed locked sea ice/surface albedo feedbacks (Graversen and Wang 2009, Graversen *et al* 2014, Merlis 2014, Dekker *et al* 2019) and aquaplanets without sea ice (Langen and Alexeev 2007, Langen *et al* 2012, Russotto and Biasutti 2020).

What mechanisms best explain the initial appearance and the subsequent evolution of AA? From an atmospheric column energy budget perspective, SHU and, to a lesser extent, the LR feedback are the dominant mechanisms by which AA develops in Jan 4 × CO₂. A similar positive contribution from the LR feedback on short timescales was also documented by Previdi *et al* (2020). Jul 4 × CO₂ shows a similar initially positive contribution to AA from SHU, but it becomes negligible in the first week. Instead, in Jul 4 × CO₂, the surface albedo feedback appears to be the leading mechanism by which AA develops on short timescales.

Upon decomposing the SHU response, we found that the difference in the Arctic and global average surface latent heat flux response produces AA on ultrafast timescales. The difference in 4 × CO₂ surface RF between the Arctic and global average further contributes to this ultrafast AA response in Jul 4 × CO₂ but is much smaller. The rapid response of the surface latent heat flux that we have documented here, which is dominated by a strong reduction in the global-mean surface evaporation, has previously been recognized as a rapid adjustment to increasing atmospheric CO₂ in studies of the global hydrological cycle (Allen and Ingram 2002, Bala *et al* 2010). However, it is our understanding that this study is the first to recognize its importance for AA.

On longer timescales (i.e., >1 month), other mechanisms become important in shaping the evolution of AA in the simulations. The most prominent contribution to AA in both Jan 4 × CO₂ and Jul 4 × CO₂ comes from the summertime surface albedo feedback; increased moisture flux convergence and water vapor feedback are additional smaller contributions to AA in the summer. Despite this, AA is absent (or very weak) during the summer months, which can be explained by the substantially negative SHU contribution and, to a lesser extent, the LR feedback. The strongly negative SHU contribution reflects the absorption of excess heat by the ocean mixed layer (mainly due to the surface albedo feedback). This excess heat is released into the atmosphere later in the year. By autumn, AA begins to strengthen and reaches its peak intensity at the end of October, with positive contributions from the Planck feedback, LR feedback, and SHU (Rigor *et al* 2002, Serreze *et al* 2009, Screen and Simmonds 2010, Stroeve *et al* 2012, Boeke and Taylor 2018, Chung *et al* 2021, Hahn *et al* 2021, Jenkins and Dai 2022).

We stress that commonly cited AA mechanisms like sea ice loss and the moisture flux convergence into the Arctic are not unimportant but rather cannot explain the ultrafast development of AA after CO₂ increase. Our results show that the leading causes of AA depend on the timescale examined, a nuance often overlooked in the existing body of AA research. Although an abrupt quadrupling of CO₂ is a highly idealized RF chosen for the purpose of this study, the evolutions of feedbacks and energy transports are likely important considerations for any study of AA mechanisms.

How does the time of year in which atmospheric CO₂ is quadrupled affect AA development? AA is slower to develop in Jul 4 × CO₂ than in Jan 4 × CO₂ (25 d vs. 1 d), hampered by an immediately negative Arctic LR feedback and a negative contribution from SHU. This result is unsurprising, given the well-known summertime minimum in AA (Lainé *et al* 2016, Previdi *et al* 2021). Despite this, robust AA forms by the end of the first month in both experiments and persists through most of the following two years. Maximum Arctic SAT increase in Jan 4 × CO₂ and Jul 4 × CO₂ occurs over land areas, further evidence that sea ice loss is not the dominant mechanism in the rapid development of AA.

It is interesting to consider whether the ultrafast SHU and LR responses documented here (i.e., those occurring in the first few days to weeks of 4 × CO₂) may be classified as rapid adjustments, which are defined as the response to an external forcing that is independent of global surface temperature change (Forster *et al* 2013). Given that the global SAT change is small on these fast timescales, the adjustment framework may be appropriate. To the extent that it is, it would suggest that AA fundamentally owes its existence to rapid adjustments, which act to enhance Arctic warming before slower components of the climate system, such as sea ice, have a chance to respond. The ultrafast response of the Arctic to RF implies the potential for significant near-term mitigation of Arctic warming if humanity acts quickly to reduce atmospheric CO₂.

Data availability statements

The data that support the findings of this study are openly available at the following URL/DOI: <https://doi.org/10.5281/zenodo.8106060>. The CESM simulations that support the findings of this study are available upon request from the authors.

Acknowledgments

The authors gratefully acknowledge the NCAR Large Ensemble Community Project and supercomputing resources provided by the National Center for Atmospheric Research Computing and Informational Systems Lab, technical support from Dr Gustavo Correa, and the insightful contributions from two anonymous reviewers.

Funding

T J, M P, K S, and L P were funded by the National Science Foundation Office of Polar Programs, Arctic Research Opportunities Grant No. PLR-1603350. T J was also funded by the National Science Foundation Graduate Research Fellowship Program, Grant No. DGE-2036197. G C was funded by the National Swiss Science Foundation Ambizione Grant No. PZ00P2_180043.

ORCID iDs

Tyler P Janoski  <https://orcid.org/0000-0003-4344-355X>
Michael Previdi  <https://orcid.org/0000-0001-7701-1849>
Gabriel Chiodo  <https://orcid.org/0000-0002-8079-6314>
Karen L Smith  <https://orcid.org/0000-0002-4652-6310>
Lorenzo M Polvani  <https://orcid.org/0000-0003-4775-8110>

References

- Allen M R and Ingram W J 2002 Constraints on future changes in climate and the hydrologic cycle *Nature* **419** 228–32
- Altdorff D, Borchard N, Young E H, Galagedara L, Sorvali J, Quideau S and Unc A 2021 Agriculture in boreal and Arctic regions requires an integrated global approach for research and policy *Agron. Sustain. Dev.* **41** 23
- Arrhenius S 1896 XXXI. On the influence of carbonic acid in the air upon the temperature of the ground *London, Edinburgh Dublin Phil. Mag. J. Sci.* **41** 237–76
- Bala G, Caldeira K and Nemani R 2010 Fast versus slow response in climate change: implications for the global hydrological cycle *Clim. Dyn.* **35** 423–34
- Banerjee A, Chiodo G, Previdi M, Ponater M, Conley A J and Polvani L M 2019 Stratospheric water vapor: an important climate feedback *Clim. Dyn.* **53** 1697–710
- Bintanja R and Kriken F 2016 Magnitude and pattern of Arctic warming governed by the seasonality of radiative forcing *Sci. Rep.* **6** 38287
- Bintanja R and van der Linden E C 2013 The changing seasonal climate in the Arctic *Sci. Rep.* **3** 1556
- Bitz C M, Gent P R, Woodgate R A, Holland M M and Lindsay R 2006 The influence of sea ice on ocean heat uptake in response to increasing CO₂ *J. Clim.* **19** 2437–50
- Boeke R C and Taylor P C 2018 Seasonal energy exchange in sea ice retreat regions contributes to differences in projected Arctic warming *Nat. Commun.* **9** 5017
- Boeke R C, Taylor P C and Sejas S A 2021 On the nature of the Arctic's positive lapse-rate feedback *Geophys. Res. Lett.* **48** e2020GL091109

- Cao Y, Liang S, Chen X, He T, Wang D and Cheng X 2017 Enhanced wintertime greenhouse effect reinforcing Arctic amplification and initial sea-ice melting *Sci. Rep.* **7** 8462
- Cardinale C J, Rose B E J, Lang A L and Donohoe A 2021 Stratospheric and tropospheric flux contributions to the polar cap energy budgets *J. Clim.* **34** 4261–78
- Chung E-S, Ha K-J, Timmermann A, Stuecker M F, Bodai T and Lee S-K 2021 Cold-season Arctic amplification driven by Arctic Ocean-mediated seasonal energy transfer *Earth's Future* **9** e2020EF001898
- Cohen J et al 2014 Recent Arctic amplification and extreme mid-latitude weather *Nat. Geosci.* **7** 627–37
- Conley A J, Lamarque J-F, Vitt F, Collins W D and Kiehl J 2013 PORT, a CESM tool for the diagnosis of radiative forcing *Geosci. Model Dev.* **6** 469–76
- Crook J A, Forster P M and Stuber N 2011 Spatial patterns of modeled climate feedback and contributions to temperature response and polar amplification *J. Clim.* **24** 3575–92
- Dai H 2021 Roles of surface albedo, surface temperature and carbon dioxide in the seasonal variation of Arctic amplification *Geophys. Res. Lett.* **48** e2020GL090301
- Dekker E, Bintanja R and Severijns C 2019 Nudging the Arctic Ocean to quantify sea ice feedbacks *J. Clim.* **32** 2381–95
- England M, Jahn A and Polvani L 2019 Nonuniform contribution of internal variability to recent Arctic sea ice loss *J. Clim.* **32** 4039–53
- Feldl N, Bordoni S and Merlis T M 2017 Coupled high-latitude climate feedbacks and their impact on atmospheric heat transport *J. Clim.* **30** 189–201
- Feldl N, Po-Chedley S, Singh H K A, Hay S and Kushner P J 2020 Sea ice and atmospheric circulation shape the high-latitude lapse rate feedback *npj Clim. Atmos. Sci.* **3** 1–9
- Feldl N and Roe G H 2013 Four perspectives on climate feedbacks *Geophys. Res. Lett.* **40** 4007–11
- Forster P M, Andrews T, Good P, Gregory J M, Jackson L S and Zelinka M 2013 Evaluating adjusted forcing and model spread for historical and future scenarios in the CMIP5 generation of climate models *J. Geophys. Res.* **118** 1139–50
- Francis J A and Vavrus S J 2012 Evidence linking Arctic amplification to extreme weather in mid-latitudes *Geophys. Res. Lett.* **39** L06801
- Gong T, Feldstein S and Lee S 2017 The role of downward infrared radiation in the recent Arctic winter warming trend *J. Clim.* **30** 4937–49
- Goosse H et al 2018 Quantifying climate feedbacks in polar regions *Nat. Commun.* **9** 1919
- Graversen R G and Burtu M 2016 Arctic amplification enhanced by latent energy transport of atmospheric planetary waves *Q. J. R. Meteorol. Soc.* **142** 2046–54
- Graversen R G and Langen P L 2019 On the role of the atmospheric energy transport in $2 \times \text{CO}_2$ -induced polar amplification in CESM1 *J. Clim.* **32** 3941–56
- Graversen R G, Langen P L and Mauritsen T 2014 Polar Amplification in CCSM4: contributions from the lapse rate and surface albedo feedbacks *J. Clim.* **27** 4433–50
- Graversen R G and Wang M 2009 Polar amplification in a coupled climate model with locked albedo *Clim. Dyn.* **33** 629–43
- Hahn L C, Armour K C, Zelinka M D, Bitz C M and Donohoe A 2021 Contributions to polar amplification in CMIP5 and CMIP6 models *Front. Earth Sci.* **9** 710036
- Held I M and Soden B J 2006 Robust responses of the hydrological cycle to global warming *J. Clim.* **19** 5686–99
- Henry M and Merlis T M 2019 The role of the nonlinearity of the Stefan–Boltzmann law on the structure of radiatively forced temperature change *J. Clim.* **32** 335–48
- Ho J 2010 The implications of Arctic sea ice decline on shipping *Mar. Policy* **34** 713–5
- Holland M M and Bitz C M 2003 Polar amplification of climate change in coupled models *Clim. Dyn.* **21** 221–32
- Huang Y, Tan X and Xia Y 2016a Inhomogeneous radiative forcing of homogeneous greenhouse gases *J. Geophys. Res.* **121** 2780–9
- Huang Y, Xia Y and Tan X 2017 On the pattern of CO_2 radiative forcing and poleward energy transport *J. Geophys. Res.* **122** 10,578–93
- Huang Y, Zhang M, Xia Y, Hu Y and Son S-W 2016b Is there a stratospheric radiative feedback in global warming simulations? *Clim. Dyn.* **46** 177–86
- Hurrell J W et al 2013 The community Earth system model: a framework for collaborative research *Bull. Am. Meteorol. Soc.* **94** 1339–60
- Hwang Y-T, Frierson D M W and Kay J E 2011 Coupling between Arctic feedbacks and changes in poleward energy transport *Geophys. Res. Lett.* **38** L17704
- Jahn A, Kay J E, Holland M M and Hall D M 2016 How predictable is the timing of a summer ice-free Arctic? *Geophys. Res. Lett.* **43** 9113–20
- Janoski T P 2023 *tyfolino/CESM-LE-Arctic-amplification: Final (Version v3)* Zenodo (<https://doi.org/10.5281/zenodo.8106060>)
- Jenkins M T and Dai A 2022 Arctic climate feedbacks in ERA5 reanalysis: seasonal and spatial variations and the impact of sea-ice loss *Geophys. Res. Lett.* **49** e2022GL099263
- Kay J E et al 2015 The Community Earth System Model (CESM) large ensemble project: a community resource for studying climate change in the presence of internal climate variability *Bull. Am. Meteorol. Soc.* **96** 1333–49
- Kay J E and Deser C 2016 The Community Earth System Model (CESM) large ensemble project *UCAR/NCAR Climate Data Gateway* (<https://doi.org/10.5065/d6j101d1>)
- Kiehl J T and Ramanathan V 1982 Radiative heating due to increased CO_2 : the role of H_2O continuum absorption in the 12–18 μm region *J. Atmos. Sci.* **39** 2923–6
- Labe Z, Magnusdottir G and Stern H 2018 Variability of Arctic sea ice thickness using PIOMAS and the CESM large ensemble *J. Clim.* **31** 3233–47
- Lainé A, Yoshimori M and Abe-Ouchi A 2016 Surface Arctic amplification factors in CMIP5 models: land and oceanic surfaces and seasonality *J. Clim.* **29** 3297–316
- Langen P L and Alexeev V A 2007 Polar amplification as a preferred response in an idealized aquaplanet GCM *Clim. Dyn.* **29** 305–17
- Langen P L, Graversen R G and Mauritsen T 2012 Separation of contributions from radiative feedbacks to polar amplification on an aquaplanet *J. Clim.* **25** 3010–24
- Lee S 2014 A theory for polar amplification from a general circulation perspective *Asia-Pac. J. Atmos. Sci.* **50** 31–43
- Manabe S and Stouffer R J 1980 Sensitivity of a global climate model to an increase of CO_2 concentration in the atmosphere *J. Geophys. Res.* **85** 5529–54
- Meltofte H, et al 2013 *Arctic Biodiversity Assessment. Synthesis* (Conservation of Arctic Flora and Fauna (CAFF)) (available at: <https://oaarchive.arctic-council.org/handle/11374/232>)
- Merlis T M 2014 Interacting components of the top-of-atmosphere energy balance affect changes in regional surface temperature *Geophys. Res. Lett.* **41** 7291–7
- Merlis T M and Henry M 2018 Simple estimates of polar amplification in moist diffusive energy balance models *J. Clim.* **31** 5811–24

- Moon T A, Druckenmiller M L and Thoman R L 2021 NOAA Arctic Report Card 2021 Executive Summary (<https://doi.org/10.25923/5S0F-5163>)
- National Snow & Ice Data Center 2020 *Arctic People* (available at: <https://nsidc.org/cryosphere/arctic-meteorology/arctic-people.html>) (Accessed 9 May 2022)
- Pendergrass A G, Conley A and Vitt F M 2018 Surface and top-of-atmosphere radiative feedback kernels for CESM-CAM5 *Earth Syst. Sci. Data* **10** 317–24
- Pithan F and Mauritsen T 2014 Arctic amplification dominated by temperature feedbacks in contemporary climate models *Nat. Geosci.* **7** 181–4
- Previdi M, Janoski T P, Chiodo G, Smith K L and Polvani L M 2020 Arctic amplification: a rapid response to radiative forcing *Geophys. Res. Lett.* **47** e2020GL089933
- Previdi M, Smith K L and Polvani L M 2021 Arctic amplification of climate change: a review of underlying mechanisms *Environ. Res. Lett.* **16** 093003
- Raval A and Ramanathan V 1989 Observational determination of the greenhouse effect *Nature* **342** 758–61
- Rigor I G, Wallace J M and Colony R L 2002 Response of sea ice to the Arctic oscillation *J. Clim.* **15** 2648–63
- Rusotto R D and Biasutti M 2020 Polar amplification as an inherent response of a circulating atmosphere: results from the TRACMIP aquaplanets *Geophys. Res. Lett.* **47** e2019GL086771
- Screen J A, Deser C, Simmonds I and Tomas R 2014 Atmospheric impacts of Arctic sea-ice loss, 1979–2009: separating forced change from atmospheric internal variability *Clim. Dyn.* **43** 333–44
- Screen J A and Simmonds I 2010 The central role of diminishing sea ice in recent Arctic temperature amplification *Nature* **464** 1334–7
- Serreze M C, Barrett A P, Stroeve J C, Kindig D N and Holland M M 2009 The emergence of surface-based Arctic amplification *Cryosphere* **3** 11–19
- Shell K M, Kiehl J T and Shields C A 2008 Using the radiative kernel technique to calculate climate feedbacks in NCAR's Community Atmospheric Model J. *Clim.* **21** 2269–82
- Singh H A, Rasch P J and Rose B E J 2017 Increased ocean heat convergence into the high latitudes with CO₂ doubling enhances polar-amplified warming *Geophys. Res. Lett.* **44** 10,583–91
- Smith D M et al 2019 The Polar Amplification Model Intercomparison Project (PAMIP) contribution to CMIP6: investigating the causes and consequences of polar amplification *Geosci. Model Dev.* **12** 1139–64
- Smith D M et al 2022 Robust but weak winter atmospheric circulation response to future Arctic sea ice loss *Nat. Commun.* **13** 727
- Soden B J, Held I M, Colman R, Shell K M, Kiehl J T and Shields C A 2008 Quantifying climate feedbacks using radiative kernels *J. Clim.* **21** 3504–20
- Stroeve J C, Serreze M C, Holland M M, Kay J E, Malanik J and Barrett A P 2012 The Arctic's rapidly shrinking sea ice cover: a research synthesis *Clim. Change* **110** 1005–27
- Stuecker M F et al 2018 Polar amplification dominated by local forcing and feedbacks *Nat. Clim. Change* **8** 1076–81
- Swart N C, Fyfe J C, Hawkins E, Kay J E and Jahn A 2015 Influence of internal variability on Arctic sea-ice trends *Nat. Clim. Change* **5** 86–89
- van der Linden E C, Le Bars D, Bintanja R and Hazeleger W 2019 Oceanic heat transport into the Arctic under high and low CO₂ forcing *Clim. Dyn.* **53** 4763–80
- Vavrus S J, Bhatt U S and Alexeev V A 2011 Factors influencing simulated changes in future Arctic cloudiness *J. Clim.* **24** 4817–30
- Wang Q, Fan X and Wang M 2016 Evidence of high-elevation amplification versus Arctic amplification *Sci. Rep.* **6** 19219
- Winton M 2006 Amplified Arctic climate change: what does surface albedo feedback have to do with it? *Geophys. Res. Lett.* **33** L03701
- Yang W and Magnusdottir G 2018 Year-to-year variability in Arctic minimum sea ice extent and its preconditions in observations and the CESM large ensemble simulations *Sci. Rep.* **8** 9070
- Zhang R, Wang H, Fu Q, Pendergrass A G, Wang M, Yang Y, Ma P-L and Rasch P J 2018 Local radiative feedbacks over the Arctic based on observed short-term climate variations *Geophys. Res. Lett.* **45** 5761–70
- Zubrzycki S, Kutzbach L and Pfeiffer E-M 2014 Permafrost-affected soils and their carbon pools with a focus on the Russian Arctic *Solid Earth* **5** 595–609